Journal of Power Sources 256 (2014) 8–13

Contents lists available at ScienceDirect

Journal of Power Sources

journal homepage: www.elsevier.com/locate/jpowsour

Complexation of polyaniline and graphene for efficient counter electrodes in dye-sensitized solar cells: Enhanced charge transfer ability

Benlin He, Qunwei Tang*, Min Wang, Chunqing Ma, Shuangshuang Yuan

Institute of Materials Science and Engineering, Ocean University of China, Qingdao 266100, Shandong Province, PR China

HIGHLIGHTS

- Aniline–graphene complexes were synthesized by a reflux technique.
- PANi–graphene complex CEs were electro-polymerized by a CV approach.
- Covalent bond between PANi and graphene can accelerate the charge transfer between them.
- A conversion efficiency of 7.70% was obtained from PANi–8 wt‰ graphene complex CE-based DSSC.

GRAPHICAL ABSTRACT

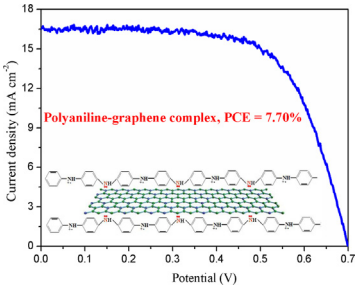

ARTICLE INFO

Article history:
Received 18 December 2013
Accepted 13 January 2014
Available online 21 January 2014

Keywords:
Dye-sensitized solar cell
Counter electrode
Polyaniline
Graphene
Complex

ABSTRACT

With an aim of significantly enhancing charge-transfer ability of counter electrodes and therefore photovoltaic performances of dye-sensitized solar cells (DSSCs), here we pioneerly report the complexation of polyaniline (PANi) and graphene as well as their employment as counter electrodes (CEs) in efficient DSSCs. Owing to the covalent bond between PANi (*N* atoms) and graphene (*C* atoms), charge transfer kinetics is dramatically elevated, which can be confirmed by the enhancement on electrocatalytic activity toward triiodides and a decrease in charge-transfer resistance. A power conversion efficiency of 7.70% is determined from DSSC using PANi–8 wt‰ graphene complex CE in comparison with 6.40% from pure PANi CE-based DSSC. The high conversion efficiency, facile charge-transfer in combination with simple preparation, relatively low cost, and scalability demonstrates the potential use of PANi–graphene complexes in robust DSSCs.

1. Introduction

Dye-sensitized solar cells (DSSCs), electrochemical devices converting solar energy into electricity, are potential solutions to energy depletion, environmental pollution, and ecological destruction [1–4]. To date, an impressive light-to-electric power conversion efficiency of 12.3% has been recorded from liquid electrolyte-based DSSC [5]. However, the commercialization of DSSCs is always obstructed by high-cost of Pt counter electrode [6]. By addressing this issue, it is a prerequisite to develop cheap CEs with honors of good electrocatalytic activity toward triiodides and rapid charge transfer ability. Conducting polymers such as polyaniline (PANi) and carbon materials such as graphene are preferred alternative CE materials [7,8]. The single use of PANi or graphene in CE always generates associated problems. For example, PANi has excellent redox behaviors but the charge-transfer ability is relatively low because of its organic semiconductor nature, whereas graphene, a single-layer material of sp^2-bond-carbon atoms in a hexagonal lattice, has an excellent electrical conduction in two dimensions, but the redox performances are unsatisfactory.

* Corresponding author. Tel./fax: +86 532 66781690.
E-mail address: tangqunwei@hotmail.com (Q. Tang).

0378-7753/$ – see front matter © 2014 Elsevier B.V. All rights reserved.
http://dx.doi.org/10.1016/j.jpowsour.2014.01.053

Previous researches are focusing on chemical, physical or electrochemical combination of PANi and graphene [9–11]. The disadvantage of the proposed approaches is relatively high interfacial resistance between PANi and graphene, which gives a low charge-transfer kinetics. The power conversion efficiencies of the DSSCs fabricated using traditional PANi–graphene CEs are in the level of ~7% [12–14].

To integrate the redox behavior of PANi and electron-conduction of graphene well, we report here the reflux synthesis of aniline–graphene complexes, in which aniline monomers are bonded onto graphene via covalent bonding between *N* atoms (electron donor) and *C* atoms (electron acceptor). The PANi–graphene complex CE electrochemically deposited on FTO conductive glass generate a promising power conversion efficiency of 7.70%, which is much higher than 6.40% from pure PANi CE-based DSSC.

2. Experimental

2.1. Reflux synthesis of aniline–graphene complexes

The aniline–graphene complexes were synthesis by a reflux process. In details, five aniline–graphene mixtures with graphene (the average diameter was around 500 nm) dosages of 1, 4, and 8 wt‰ were sealed in a three-neck flask filled with high-purity N_2 gas. In dark, the mixtures were refluxed for 6 h at 184 °C to obtain the target aniline–graphene complexes.

2.2. Deposition of PANi-graphene complex CEs

The fabrication of PANi–graphene complex CEs was on an electrochemical workstation (CHI660E): In details, a cleaned fluorine doped tin oxide (FTO, 12 Ω sq^{-1}) glass was used a working electrode, a Pt plate was a CE, and an Ag/AgCl was a reference electrode. The supporting electrolyte was 0.5 M H_2SO_4 aqueous solution dissolved aniline–graphene complex. A cyclic voltammetric method was employed at a sweep rate of 200 mV s^{-1} for 50 repeating cycles. After deposition, the electrodes were washed several times in 0.5 M H_2SO_4 aqueous solution and deionized water, dried in vacuum at 60 °C for 24 h. As a comparison, PANi-only CE was also prepared under the same synthesis conditions.

As references, Pt (purchased from Dalian HeptaChroma SolarTech, Co., Ltd, China), pure PANi, pure graphene, and PANi–8 wt‰ graphene mixture CEs were also performed under the same conditions. The synthesis of PANi CE was similar to that of PANi–graphene complex CEs. The supporting electrolyte was 0.5 M H_2SO_4 aqueous solution dissolved 0.1 mol of aniline. Graphene CE was prepared by dissolving graphene in 12.5 g L^{-1} of polyvinyldifluoride in N-methyl-2-pyrrolidone (mass ratio of graphene to polyvinyldifluoride was 95:5) and casting onto a cleaned FTO glass substrate. The film thickness was controlled at around 3 μm, then the coated FTO substrate was vacuumly dried at 60 °C for 24 h. Similarly, the PANi–8 wt‰ graphene mixture CE was also prepared according to the above procedures.

2.3. Assembly of DSSCs

A layer of TiO_2 nanocrystal anode film with a thickness of 10 μm was prepared by a sol-hydrothermal method and casted onto a cleaned FTO glass substrate. After being calcined at 450 °C for 30 min, the resultant TiO_2 films were further sensitized by immersing into a 0.5 mM ethanol solution of N719 dye (purchased from DYESOL LTD). The DSSC was fabricated by combining the dye-sensitized TiO_2 anode and FTO supported PANi–graphene complex CEs. A redox electrolyte consisted of 100 mM of tetraethylammonium lodide, 100 mM of tetramethylammonium iodide, 100 mM of tetrabutylammonium iodide, 100 mM of NaI, 100 mM of KI, 100 mM of LiI, 50 mM of I_2, and 500 mM of 4-tert-butyl-pyridine in 50 ml acetonitrile.

2.4. Electrochemical characterizations

The cyclic voltammetry (CV) curves were recorded in a supporting electrolyte consisting of 50 mM LiI, 10 mM I_2, and 500 mM $LiClO_4$ in acetonitrile. Electrochemical impedance spectroscopy (EIS) measurements were also carried out in a frequency range of 0.01 Hz ~ 10^5 kHz and an ac amplitude of 10 mV at room temperature. Tafel polarization curves were recorded by assembling symmetric cell consisting of FTO–PANi–graphene complex|liquid electrolyte|FTO-PANi–graphene complex.

2.5. Photovoltaic test

The photovoltaic test of the DSSC was carried out by measuring the current–voltage (*J–V*) characteristic curves using an Electrochemical Workstation (CHI660E, Shanghai Chenhua Device Company, China) under irradiation of a simulated solar light from a xenon-mercury arc lamp (CHF-XM-500W, Beijing Trusttech Co., Ltd) in ambient atmosphere. The incident light intensity was calibrated using an FZ-A type radiometer from Beijing Normal University Photoelectric Instrument Factory to control it at 100 mW cm^{-2} (AM 1.5). Each DSSC device was measured five times to eliminate experimental error and a compromise *J–V* curve was employed. The fill factor (*FF*) and light-to-electric energy conversion efficiency (η) was calculated according to the equations:

$$FF = \frac{P_{max}}{J_{SC} \times V_{OC}} = \frac{J_{max} \times V_{max}}{J_{SC} \times V_{OC}} \quad (1)$$

$$\eta(\%) = \frac{P_{max}}{P_{in}} \times 100\% = \frac{J_{SC} \times V_{OC} \times FF}{P_{in}} \times 100\% \quad (2)$$

where J_{SC} is the short-circuit current density (mA cm^{-2}), V_{OC} is the open-circuit voltage (V), P_{in} is the incident light power, P_{max} is the maximum power output, J_{max} (mA cm^{-2}) and V_{max} (V) are the current density and voltage at the point of maximum power output in the *J–V* curves, respectively. The relative humidity is around 25%.

2.6. Other characterizations

The morphologies of the resultant PANi or PANi–graphene complex CEs were observed with a scanning electron microscope (SEM, S4800). Fourier transform infrared spectrometry (FTIR) spectra were recorded on a PerkinElmer spectrum 1760 FTIR spectrometer by an ATR model. The UV–vis spectra were measured on a UV-3200 spectrophotometer by dissolving the samples in acetone. The fluorescence emission spectra were recorded at room temperature using a Fluorolog3-P spectrophotometer. The emission spectrum was collected using a conventional setup at excitation wavelengths of 500 nm.

3. Results and discussion

UV–vis adsorption spectra of graphene, aniline, aniline–8wt ‰ graphene mixture, and aniline–graphene complexes with various graphene dosages were diluted in acetone to reveal the complexing mechanism of aniline molecules onto graphene. As is shown in Fig. 1a, no peak is observed in the UV–vis spectrum ranging from 350 to 700 nm. In comparison with the UV–vis spectrum of aniline–graphene mixture, new absorption peaks at 366, 452, 513, and 554 nm are observed, suggesting the successful complexation of

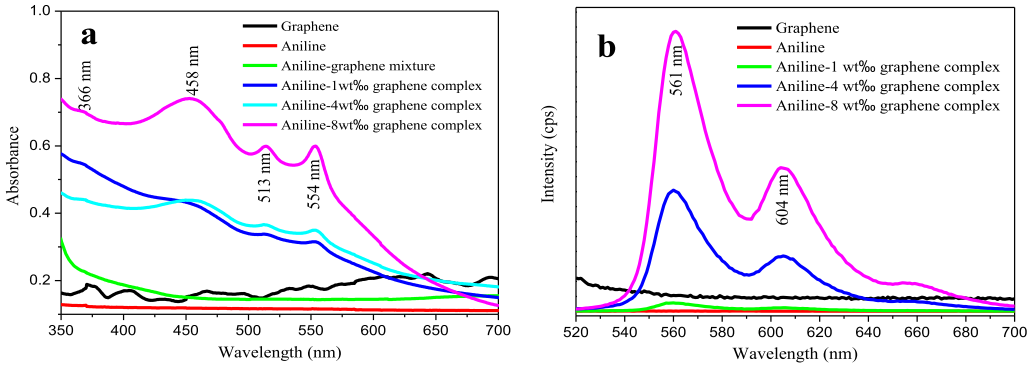

Fig. 1. (a) UV–vis absorption spectra and (b) emission spectra of pure graphene, pure aniline, aniline–8 wt‰ graphene mixture and aniline–graphene complexes diluted in acetone at graphene dosages of 1, 4, and 8 wt‰. The excitation wavelength was 500 nm.

aniline and graphene charge-transfer complex [15,16]. At elevated temperature, such as 184 °C, graphene and aniline are believed to form a facile charge-transfer complex in its ground state because graphene is a good electron acceptor, whereas aniline is a fairly good electron donor, as evidenced by the appearance of the new absorptions. During an electrochemical polymerization of PANi–graphene, each imine group (–NH–) has a lone-electron pair which can share with a carbon atom in conjugation structure of graphene (–C=) to form a covalent bond. There is a consensus that the chemical bonding between PANi and graphene can significantly accelerate the charge transfer [17]. Moreover, covalent bonding of PANi onto graphene can increase the well-aligned arrangement of PANi chains [18], resulting in high electron delocalization, long-range charge transfer and therefore good electrochemical performances. From fluorescence emission spectra in Fig. 1b, one can see that the maximum emissions in acetone are at around 561 and 604 nm, whereas the fluorescence spectra of graphene and pure aniline are generally markedly quenched. The fluorescence excitation spectra of the aniline–graphene complexes are quite different from the absorption spectra of the individual components, indicating the formation of a new light-absorbing species.

The electrochemically polymerized PANi is composed of nanofibers, as shown in Figs. 2a and b, which is a common microstructure. However, spreading structure is detected in PANi–8 wt‰ graphene complex (Fig. 2c and d), indicating that PANi has bonded onto graphene with no interfacial separation. The close covalent bonding is expected to enhance charge transfer between PANi and graphene.

Fig. 3 provides the reference FTIR spectrum of bared PANi and PANi–graphene complexes. The main absorption bands situated at ca. 886, 1177, 1310, 1512, and 1656 cm^{-1} are attributed to the following vibration modes: bending of C–H (out-of-plane) on benzene ring (B), bending of C–H (in-plane), mode of N = quinoid ring (Q) = N, stretching of Caromatic-N, stretching of N–B–N and stretching of N=Q=N, respectively [19,20]. By comparison with bared PANi spectrum, the FTIR spectra of PANi–graphene complex give a signal of appearance of the 1053 cm^{-1} band, especially in high graphene dosage. The present of this FTIR band indicates a charge transfer and a selective interaction of the graphene fragments with quinoid rings of PANi backbones [21]. A similar interaction between carbon nanotubes and PANi quinoid rings has also been detected in PANi/multi-walled CNTs [22]. The band attributed

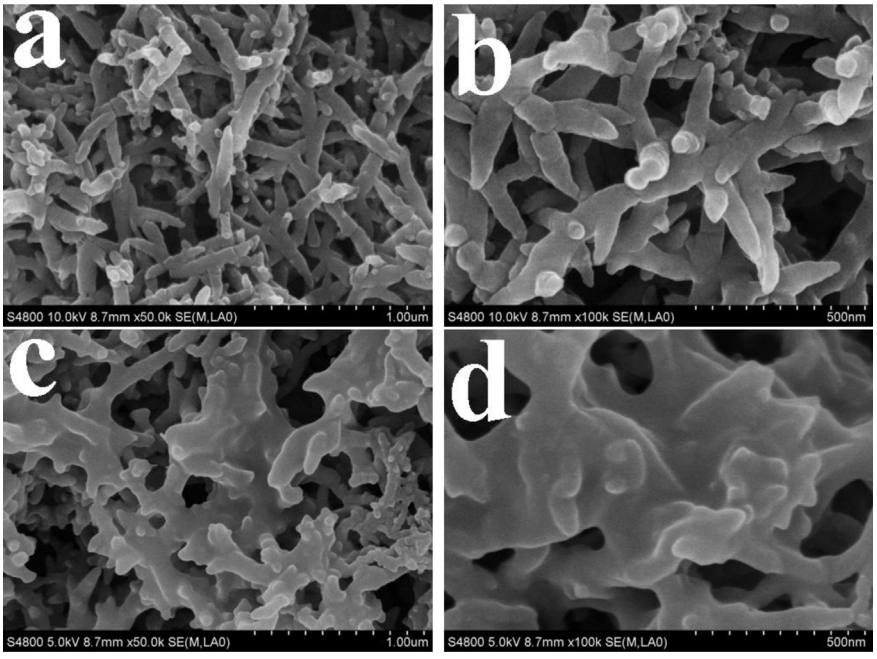

Fig. 2. SEM photographs of (a) & (b) PANi and (c) & (d) PANi–8 wt‰ graphene complex CEs.

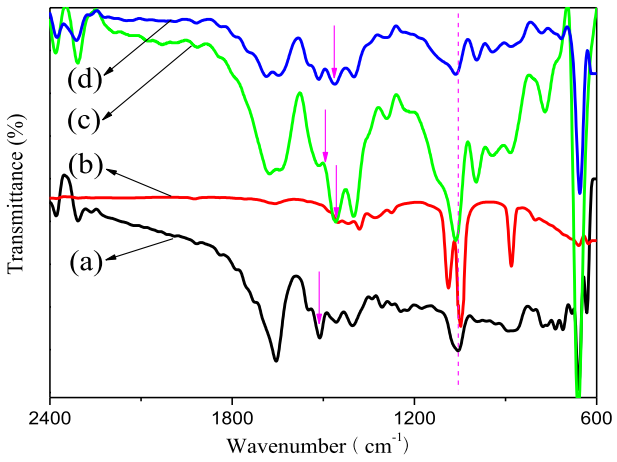

Fig. 3. FTIR spectra of (a) PANi, (b) PANi–1 wt‰ graphene, (c) PANi–4 wt‰ graphene, and (d) PANi–8 wt‰ graphene complexes.

to N–B–N stretching has been shifted from 1512 cm^{-1} to 1450, 1497, and 1467 cm^{-1} in PANi–1 wt‰ graphene complex, PANi–4 wt‰ graphene complex, and PANi–8 wt‰ graphene complex, respectively. The band shift maybe the result of vibration restriction in forming covalent bond between –NH– (PANi) and –C= (graphene).

The CV curves of the resultant complex CEs in liquid electrolyte with PANi-only CE as a reference was recorded, as is shown in Fig. 4a. The peak positions and shapes of the CV curves from PANi–graphene complex CEs are very similar to those of Pt and PANi-only CE [23], revealing that PANi–graphene complex CEs have a similar electrocatalytic activity to Pt CE. Considering that the task of CE is to reduce redox species, mediators in regenerating the sensitizer after electron injection in a liquid-state DSSC, the electroreduction reaction of $I_3^- + 2e \rightarrow 3I^-$ can be employed to elevate the electrocatalytic activity of PANi–graphene complex CEs. It is noteworthy to mention that the PANi–8 wt‰ graphene complex CE has the highest electrocatalytic activity toward triiodide reduction. The increase in bonding sites between PANi and graphene has a promotion effect on electrocatalytic performance of PANi–graphene complex CE, however, much higher graphene dosage such as higher than 8 wt‰, is expected to provide low ratio of complexes replaced by disordered graphene aggregations, blocking the rapid charge transfer between PANi and graphene. As a comparison, the CV curves of Pt, PANi, grapheme, and PANi–8 wt‰ graphene mixture CEs were also determined and shown in Fig. 4a. Apparently, the densities of their J_{red1} peaks are all lower than that of PANi–graphene complex CEs. Moreover, the ratio of $J_{ox1}/|J_{red1}|$ is a parameter to elevate the reversibility of the redox reaction toward I^-/I_3^- [24]. The obtained values from PANi, PANi–1 wt‰ graphene, PANi–4 wt‰ graphene, and PANi–8 wt‰ graphene complex CEs are 1.14, 0.93, 0.94, and 0.95, respectively. The closer $J_{ox1}/|J_{red1}|$ from PANi–8 wt‰ graphene complex CE to 1.0 indicates a more reversible redox reaction for $I_3^- \leftrightarrow I^-$. The rapid recovery of iodides to their ground state facilitates the participation in subsequent circles and improves the long-term stability. To elucidate the relationship between increased bonding sites and diffusion of iodide in a complex CE, Randles-Sevcik theory is employed and presented [25]:

$$J_{red} = Kn^{1.5}ACD_n^{0.5}v^{0.5} \quad (3)$$

where J_{red} is the peak current density of Red_1 (mA cm^{-2}), K is 2.69×10^5, n is the number of electrons of reduction reaction, A is the electrode area (cm^2), C represents the bulk concentration of I_3^-

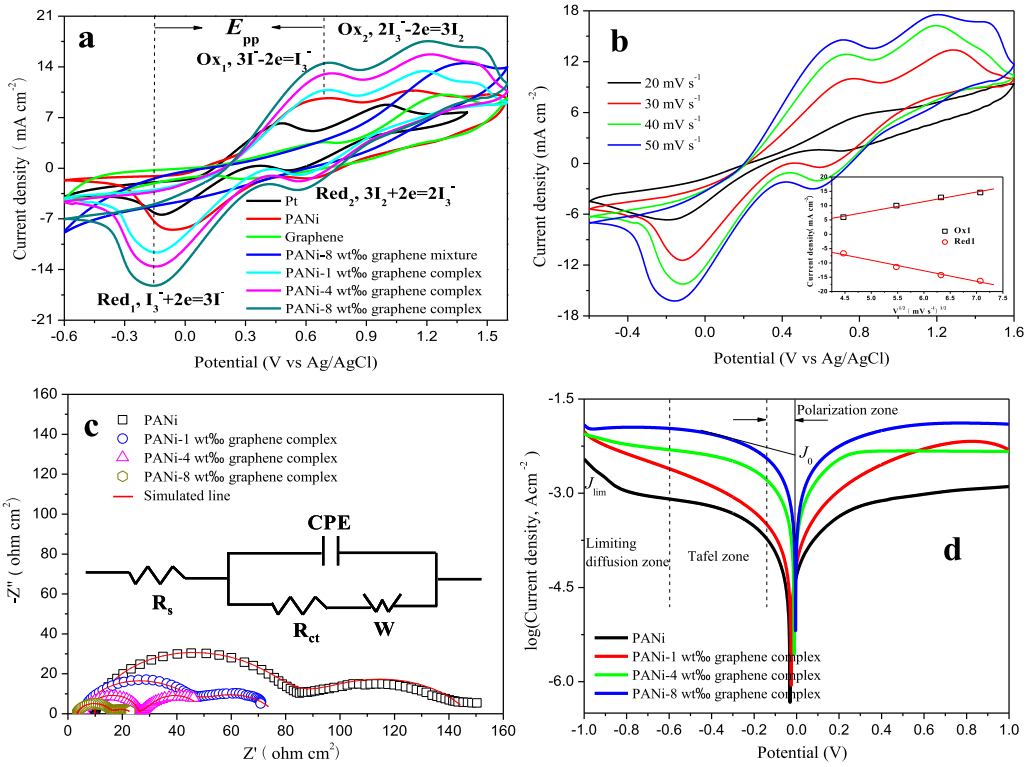

Fig. 4. (a) CV curves of PANi, graphene, Pt, PANi–8 wt‰ graphene mixture and PANi–graphene complex CEs for I^-/I_3^- redox species recorded at a scan rate of 50 mV s^{-1}. (b) CV curves of PANi–8 wt‰ graphene complex CE for I^-/I_3^- redox species at varied scan rates (from inner to outer: 20, 30, 40, and 50 mV s^{-1}), and (b) relationship between peak current density and square root of scan rates. (c) Nyquist plots and (d) Tafel polarization curves for symmetric cells fabricated with PANi-only or PANi–graphene complex CEs. The lines express fit results for corresponding EIS data, and the inset gives the equivalent circuit.

(mol L^{-1}), D_n is the diffusion coefficient (cm^{-2} s^{-1}). The diffusivity of PANi-only CE is 3.09×10^{-5} cm^{-2} s^{-1} which is comparable to 4.92×10^{-6} cm^{-2} s^{-1} of poly(3,4-ethylenedioxythiophene) (PEDOT) and 2.55×10^{-6} cm^{-2} s^{-1} of Pt CEs [26]. Interestingly, D_n is 2.56×10^{-5}, 6.65×10^{-5}, and 1.86×10^{-4} cm^{-2} s^{-1} for PANi–1 wt‰ graphene complex, PANi–4 wt‰ graphene complex, and PANi–8 wt‰ graphene complex, respectively. The results indicate that the enhanced bonding sites between PANi and graphene can accelerate both charge transfer and iodide species within PANi–-graphene complex CEs.

From the stacking CV curves of PANi–8 wt‰ graphene complex CE at different scan rates, one can find an outward extension of all the peaks (Fig. 4b). By plotting peak current density corresponding to $I_3^- \leftrightarrow I^-$ versus square root of scan rate, as shown in insert of Fig. 4b, linear relationships are observed. This result indicates the redox reaction on the surface of the PANi–8 wt‰ graphene complex CE is controlled by ionic diffusion in the electrolyte, and the transfer rate of both electrons and ions are fast enough for the reduction rate of I_3^- on the surface of PANi–8 wt‰ graphene complex CE. This result also suggests that the adsorption of iodide species is hardly affected by the redox reaction on the PANi–8 wt‰ graphene complex CE surface and no specific interaction occurred between I^-/I_3^- and the CE [27].

In order to understand the impressive improvement on electrocatalytic activity, EIS experiments were carried out with dummy cells fabricated with two identical electrodes. Fig. 4c presents the EIS results of PANi and PANi–graphene complex CEs in the form of Nyquist plots. Two semicircles are detected in each EIS plot, which represent two different steps of reaction in the electrochemical process. The left semicircle at high-frequency region is correlated to charge-transfer resistance (R_{ct}) and the corresponding chemical capacitance (CPE) of the electrode/electrolyte interface, while the right semicircle at low-frequency region refers to the Nernst diffusion impedance (W). A series resistance (R_s), mainly composed of bulk resistance of CE material [28], resistance of FTO layer and the contact resistance of FTO/electrode, is also included in the equivalent circuit and can be obtained from the high frequency intercept on the real axis. The R_{ct} of the dummy cell is estimated by taking half value of the diameter of its corresponding semicircle. From the output in Table 1, there is a slight decrease of R_s value, which is responsible for the enhanced charge-transfer ability of PANi–graphene complex at high graphene dosage. Moreover, the high-frequency semicircle shrinks clearly from PANi–8 wt‰ graphene complex CE to pure PANi CE. This means the diffusion of the redox couples within the complex is accelerated by the active sites. Especially, the remarkable difference in EIS fitting data is that the R_{ct} of PANi–8 wt‰ graphene complex CE (18.97 Ω cm^2) is almost five times smaller than that of pure PANi CE (92.91 Ω cm^2). The order of R_{ct} is PANi–8 wt‰ graphene complex < PANi–4 wt‰ graphene complex < PANi–1 wt‰ graphene complex < PANi. Since R_{ct} varies inversely with the electrocatalytic activity for the reduction of I^-/I_3^- redox species [29], such enormous decrease demonstrates that the PANi–8 wt‰ graphene complex CE has the highest electrocatalytic activity. The conclusions for the electrocatalytic activity and diffusion derived from EIS and CV data are consistent. Tafel polarization curves were also confirmed with the dummy cells similar to those in EIS measurements to verify the electrocatalytic activities and charge transfer of CEs. Fig. 4d displays the Tafel curves with logarithmic current density (log J) as a function of the voltage. Theoretically, the Tafel curve can be divided into three zones [30]. The curve at very high potential is attributed to the limiting diffusion zone, which depends on the transport of triiodide and iodide in the electrolyte. The curve at relatively low potential but higher than 120 mV corresponds to the Tafel zone, where the voltage is a linear function of log J. The curve at very low potential is polarization zone, arising from the electrochemical reaction. The larger slope for the anodic or cathodic branch in Tafel polarization curves indicates a higher exchange current density (J_0) on the electrode and better catalytic activity toward triiodide reduction. As shown in Fig. 4d, the J_0 follows an order of PANi–8 wt‰ graphene > PANi–4 wt‰ graphene > PANi–1 wt‰ graphene > PANi, which matches the order of R_{ct} because J_0 is associated with the R_{ct} by the equation [31]:

$$J_0 = RT/nFR_{ct} \quad (4)$$

where R is the universal gal constant, T is the absolute temperature, n is the number of electrons contributing to the charge transfer at the interface, and F is Faraday's constant. Therefore, the EIS and Tafel results match well.

Fig. 5 shows the photovoltaic characteristics of DSSCs employing pure PANi and PANi–graphene complex CEs under an illumination intensity of 100 mW cm^{-2} from an AM 1.5G solar simulator. The related photovoltaic parameters are summarized in Table 1, which reveals that DSSCs using PANi–graphene complex CEs shows enhanced photovoltaic efficiency when compared with that of pure PANi. In particular, the DSSC from PANi–8 wt‰ graphene CE displays short-circuit current density (J_{sc}), open circuit voltage (V_{oc}),

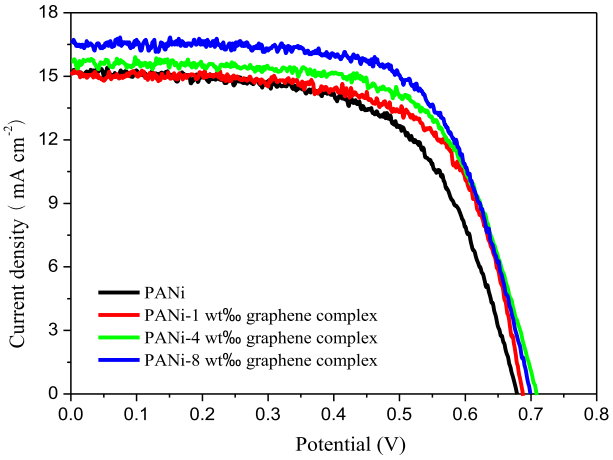

Fig. 5. J–V characteristics of DSSCs from pure PANi and PANi–graphene complex CEs.

Table 1
Parameters for equivalent circuit obtained by fitting EIS data using a Z-view software and for DSSC devices.

CEs	EIS data			DSSC data			
	R_s (Ω cm^{-2})	R_{ct} (Ω cm^{-2})	W (Ω cm^{-2})	J_{sc} (mA cm^{-2})	V_{oc} (V)	FF	η (%)
PANi	9.73	64.46	73.35	15.21	0.678	0.62	6.40
PANi–1 wt‰ graphene complex	6.98	36.56	34.21	15.23	0.687	0.66	6.93
PANi–4 wt‰ graphene complex	5.39	18.56	23.68	15.73	0.708	0.65	7.25
PANi–8 wt‰ graphene complex	3.45	11.49	8.76	16.55	0.699	0.67	7.70

R_s: series resistance; R_{ct}: charge-transfer resistance; CPE: a constant phase element; W: Nernst diffusion impedance; J_{sc}: short-circuit current density; V_{oc}: open-circuit voltage, FF: fill factor; η: power conversion efficiency.

and fill factor (*FF*) of 16.55 mA cm^{-2}, 0.699 V, and 0.67, respectively, generating its power conversion efficiency of 7.70%, which is superior to 6.40% for the pure PANi electrode. All the DSSCs are constructed from the same photoanode and liquid electrolyte, which are the predominant origins accounting for the deviation in photovoltaic performances. Therefore, the recorded V_{oc} values are also similar. The DSSCs employing PANi–graphene complex CEs achieve higher J_{sc} than that fabricated using a PANi-only CE. This might be attributed to the good dispersion of PANi–graphene complexes, which provides larger active surface areas for triiodides reduction. Moreover, the elevated amounts of active sites for PANi–8 wt‰ graphene CE can accelerate the recovery of triiodides and therefore promote electron-transfer kinetics, which may be another factor in enhancing the photocurrent density of a DSSC. The PANi–graphene complex, prepared at the optimal condition in this study, significantly improves the charge-transfer ability within CEs, which is evident in the higher J_{sc} observed for the DSSCs. After performing a comprehensive analysis of the DSSCs, it can be concluded that the photovoltaic performance is in an agreement with CV, EIS and Tafel polarization results.

4. Conclusions

In conclusion, we have demonstrated that fabrication of PANi–graphene complex CEs by a reflux technique is an effective strategy for accelerating the charge transfer within the complexes. New light-absorbing species and absorption bands can be detected from the fluorescence excitation and UV–vis absorption spectra of aniline–graphene complexes. Covalent bonds between PANi (–NH–) and graphene (–C═) are expected to significantly accelerate the charge transfer. The DSSC employing PANi–8 wt‰ graphene complex CE provides an impressive power conversion efficiency of 7.70% in comparison with 6.40% from pure PANi CE-based DSSC. The research presented here is far from being optimized but these profound advantages along with low-cost synthesis and scalable materials promise the new PANi–graphene complex CEs to be strong candidates in robust DSSCs.

Acknowledgments

The authors gratefully acknowledge Ocean University of China for providing Seed Fund to this project, and Fundamental Research Funds for the Central Universities (201313001, 201312005), Shandong Province Outstanding Youth Scientist Foundation Plan (BS2013CL015), Doctoral Fund of Ministry of Education of China (20130132120023), Shandong Provincial Natural Science Foundation (ZR2011BQ017), and Research Project for the Application Foundation in Qingdao (13-1-4-198-jch).

References

[1] B. O'Regan, M. Grätzel, Nature 353 (1991) 737–740.
[2] U. Bach, D. Lupo, P. Comte, J.E. Moser, F. Weissortel, J. Salbeck, M. Grätzel, Nature 395 (1998) 583–585.
[3] M. Grätzel, Nature 414 (2001) 338–344.
[4] Q.W. Tang, H.Y. Cai, S.S. Yuan, X. Wang, J. Mater. Chem. A 1 (2013) 317–323.
[5] A. Yella, H.W. Lee, H.N. Tsao, C. Yi, A.K. Chandiran, M.K. Nazeeruddin, E.W. Diau, C.Y. Yeh, S.M. Zakeeruddin, M. Grätzel, Science 334 (2011) 629–634.
[6] S. Yun, L. Wang, W. Guo, T.L. Ma, Electrochem. Commun. 24 (2012) 69–73.
[7] Q.H. Li, J.H. Wu, Q.W. Tang, Z. Lan, P.J. Li, J.M. Lin, L.Q. Fan, Electrochem. Commun. 10 (2008) 1299–1302.
[8] G.Q. Wang, W. Xing, S.P. Zhuo, Electrochim. Acta 92 (2013) 269–275.
[9] G.Q. Wang, W. Xing, S.P. Zhuo, Electrochim. Acta 66 (2012) 151–157.
[10] W. Sun, T. Peng, Y. Liu, S. Xu, J. Yuan, S. Guo, X.Z. Zhao, J. Mater. Chem. A 1 (2013) 2762–2768.
[11] T. Remyamol, H. John, P. Gopinath, Carbon 59 (2013) 308–314.
[12] H. Sun, Y. Luo, Y. Zhang, D. Li, Z. Yu, K. Li, Q.B. Meng, J. Phys. Chem. C. 114 (2010) 11673–11679.
[13] C.Y. Liu, K.C. Huang, P.H. Chung, C.C. Wang, C.Y. Chen, R. Vittal, C.G. Wu, W.Y. Chiu, K.C. Ho, J. Power Sources 217 (2012) 152–157.
[14] G.Q. Wang, S.P. Zhuo, W. Xing, Mater. Lett. 69 (2012) 27–29.
[15] Y. Sun, S.R. Wilson, D.I. Schuster, J. Am. Chem. Soc. 123 (2001) 5348–5349.
[16] Z.S. Qian, C. Wang, H. Feng, C.C. Chen, J. Zhou, J.R. Chen, Chem. Commun. 47 (2011) 7167–7169.
[17] M.A. Bavio, G.G. Acosta, T. Kessler, J. Power Sources 245 (2014) 475–481.
[18] C.D.G. Minto, A.S. Vaughan, Polymer 38 (1997) 2683–2688.
[19] J. Wu, Q. Tang, Q. Li, J. Lin, Polymer 49 (2008) 5262–5267.
[20] Q. Tang, J. Wu, X. Sun, Q. Li, J. Lin, L. Fan, Polymer 50 (2009) 752–755.
[21] M. Baibarac, I. Baltog, C. Godon, S. Lefrant, O. Chauvet, Carbon 42 (2004) 3143–3152.
[22] M. Cochet, W.K. Maser, A.M. Benito, M.A. Callejas, M.T. Martinez, J.M. Benoit, et al., Chem. Commun. (2001) 1450–1451.
[23] Z.Y. Tang, J.H. Wu, M. Zheng, J.H. Huo, Z. Lan, Nano Energy 2 (2013) 622–627.
[24] H. Tributsch, Coord. Chem. Rev. 248 (2004) 1511–1530.
[25] T. Daeneke, A.J. Mozer, T.H. Kwon, N.W. Duffy, A.B. Holmes, U. Bach, L. Spiccia, Energy Environ. Sci. 5 (2012) 7090–7099.
[26] Y.M. Xiao, J.Y. Lin, S.Y. Tai, S.W. Chou, G.T. Yue, J.H. Wu, J. Mater. Chem. 22 (2012) 19919–19925.
[27] Y. Saito, W. Kubo, T. Kitamura, Y. Wada, S. Yanagida, J. Photochem. Photobiol. A 164 (2004) 153–157.
[28] L. Kavan, J.H. Yum, M. Grätzel, ACS Nano 5 (2011) 165–172.
[29] L.C. Chen, K.J. Lee, J.H. Chen, T.C. Pan, C.M. Huang, Electrochim. Acta 112 (2013) 698–705.
[30] G. Wang, S. Kuang, D. Wang, S. Zhuo, Electrochim. Acta 113 (2013) 346–353.
[31] M. Wu, X. Lin, Y. Wang, L. Wang, W. Guo, D. Qi, et al., J. Am. Chem. Soc. 134 (2012) 3419–3428.